Computational characterization of micro- to macroscopic mechanical behavior and damage of polymers containing second-phase particles

Tomita, Yoshihiro

Wei, Lu

(Citation)
International Journal of Damage Mechanics,11(2):129-149

(Issue Date)
2002-04

(Resource Type)
journal article

(Version)
Accepted Manuscript

(URL)
https://hdl.handle.net/20.500.14094/90000021

Computational Characterization of Micro- to Macroscopic Mechanical Behavior and Damage of Polymers Containing Second-Phase Particles

Yoshihiro Tomita and Wei Lu
Graduate School of Science and Technology,
Kobe University, Nada, Kobe, Japan 657-8501
Fax: +81-78-803-6125 Email: tomita@mech.kobe-u.ac.jp

Abstract

To clarify the mechanical characteristics and damage of polymers containing second-phase particles, i.e., blended polymers, a homogenization method has been developed which can handle the large deformation problems, including onset and propagation of instability, and completely reproduce the periodic feature of the distribution of second-phase particles under any macroscopically homogeneous loading condition. The parametric study has clarified the characteristic features of polymers containing periodically distributed soft cylindrical particles of different volume fractions and sizes subjected to macroscopically homogeneous stress in different directions. The results indicate that, depending on the tensional direction with respect to the unit cell, different types of shear bands are observed, and that the shear band connecting the particles that appeared in the early stages of deformation is responsible for the reduction of the macroscopic yield stress. Increasing the volume fraction of particles causes a decrease of the macroscopic yield stress and of the directional dependence of the macroscopic stress-strain relation. The size difference of particles causes very complicated and different types of shear bands, however, due to the high stress concentration caused by the presence of small particles, the onset and propagation of shear bands are promoted, and the macroscopic deformation behaviors become essentially isotropic. The maximum mean stress appears in the small particle, which suggests that the blending of particles of different sizes promotes the onset of cavitation, which suppresses the maximum mean stress in the matrix and results in additional shear deformation and in preventing onset of damage in matrix caused by crazing. The location of maximum normal stress on the boundary surface between particles and matrix moves with the propagation of the shear band. The magnitude of maximum normal stress increases with the increase of the size difference between the particles and with the decrease of the volume fraction within the present simulation.

Key words: Computational Simulation, Homogenization Method, Blended Polymer, Damage of Polymer, Molecular Chain Network Model, Onset and Propagation of Instability, Periodically Distributed Particles.

Running headline: Mechanical Behavior and Damage of Blended Polymers

1. Introduction

Blending of a 10 to 40% volume fraction of second-phase particles having sizes in the range of 0.1 up to 10 μm is commonly adopted to control the mechanical properties of a polymer. It has been clarified experimentally that the cavitation of second-phase particles, conventionally rubber particles, is a key step in the toughening mechanism of polymers (Yee, 1977, Fukui et al. 1991, The Society of Polymer Science, Japan, 1991). This cavitation leads to a porous matrix in which triaxiality next to the void is substantially decreased, which suppresses the onset of damage due to crazing and promotes plastic shear deformation in the materials (Steenbrink and Van der Giessen, 1997). As a result, energy dissipation due to plastic deformation is considerably enhanced.

In order to clarify the deformation behaviors of blended polymers, computational studies have been performed. Initial studies were on simulations employing the constitutive equation of elastoplastic materials for matrix polymers so that the complicated nature of the deformation behavior of matrix polymers was not accurately reproduced. The realistic constitutive equations for polymeric materials were established in the late 1980s and modified and generalized to accurately reproduce experimentally observed evidence. Among them are three-chains model (Boyce et al. 1988), eight-chains model (Arruda and Boyce, 1993) and continuously distributed chain model (Wu and Van der Giessen 1993) in which the number of entangled points of molecular chains is unchanged during the deformation processes. These are referred to as affine models. Subsequently, to accommodate the experimentally observed evidence that suggests a change in the number of entanglement points (Raha and Bowden, 1972, Botto et al. 1987) and nonassociativeness of the strain rate with respect to the driving stress (Kashu et al. 1996, Adachi et al. 1998), the nonaffine model (Tomita et al. 1997, Tomita and Adachi 1998) and nonassociative model (Tomita et al. 1999) have been developed. Therefore, quantitative simulation of the blended polymers using the developed constitutive equations has become possible. The computational simulations employing more realistic constitutive equations have been carried out (Steenbrink and Van der Giessen, 1997, Tanaka et al. 2000, Socrate and Boyce, 2000, Steenbrink and van der Giessen, 1998, 1999, Smit et al. 1999) and the mechanisms of the improvement of mechanical characteristics of polymers upon blending the second-phase particles, i.e., rubber particles, have been investigated. However, a computational study of the blended materials, which employs the proper constitutive equation of the polymer, is restricted to the unit cell deformed under simple loading processes (Steenbrink and Van der Giessen, 1997, Tanaka et al. 2000, Socrate and Boyce, 2000, Steenbrink and van der Giessen, 1998). The representative volume element method was employed for a large number of voids with random distribution and mainly discussed the effect of the volume fraction and distribution of voids on the macroscopic response (Smit et al. 1999).

To clarify the mechanical aspect and provide a quantitative picture with respect to the mechanisms of improvement of the mechanical characteristics of the blended materials, the

homogenization method for the linear elastic problem (Guedes and Kikuchi, 1990) is extended to large-deformation problems including onset and propagation of instability. The method can completely reproduce the periodic feature of the distribution of blended material under any macroscopically homogeneous loading condition. The parametric study has been performed by means of a series of simulations for a plane strain glassy polymer, containing periodically distributed cylindrical inclusions of different volume fractions and sizes, subjected to macroscopically homogeneous stress in different directions with respect to the periodically distributed particles.

2. Constitutive Equations

To describe the experimentally observed characteristic feature of the glassy polymers, the molecular chain network model has been established, in which the microstructure of a glassy polymer is assumed to consist of long molecular chains, which are randomly distributed in space. A single chain, which consists of several segments containing monomers, is defined by two cross-links, which are assumed to be physically entangled points of molecular chains and their numbers are assumed to remain constant during deformation. These results in a network-like structure, as in rubber, but with the chemical cross-links replaced by physical entanglements. According to the theory proposed by Harward and Thackray (1968), the glassy polymer must overcome two physically distinct resistances before large-strain inelastic flow may occur. Below the glass transition temperature, prior to the initial yield, the material must be stressed to exceed its intermolecular resistance to segment rotation. Once the material is free to flow, molecular alignment occurs and results in an anisotropic internal resistance to further inelastic deformation, which is referred to as orientation hardening.

The intermolecular resistance to plastic flow is considered to be due to the impedance imposed by neighboring chains on the ability of a chain segment to rotate. Based on the assumption that plastic flow occurs due to double kinking of molecular chains, Argon (1973) developed the constitutive equation for the plastic shear strain rate, $\dot{\gamma}^p$:

$$\dot{\gamma}^p = \dot{\gamma}_0 \exp\left[\left(-\frac{As_0}{T}\right)\left\{1-\left(\frac{\tau}{s_0}\right)^{5/6}\right\}\right], \tag{1}$$

where $\dot{\gamma}_0$ and A are constants, T is the absolute temperature, $s_0 = 0.077G/(1-\nu)$ is the athermal shear strength, G is the elastic shear modulus, ν is Poisson's ratio and τ is the applied shear stress. Boyce et al. (1988) extended this expression to include the effect of pressure. They used $s+ap$ instead of s_0, where s is the shear strength which changes with plastic strain from s_0 to a stable value s_{ss}, p is the pressure and a is a pressure-dependent coefficient. Since s depends on the temperature and strain rate, the evolution equation of s can be expressed as $\dot{s} = h\left\{1-\left(s/s_{ss}\right)\right\}\dot{\gamma}^p$ where h is the rate of

resistance with respect to plastic strain.

When a polymeric material experiences a stress that exceeds its intermolecular resistance, molecular chain alignment occurs. This alignment generates back-stress, which is expressed based on the molecular chain network theory. The principal components of the back-stress tensor for the eight-chain model (Arruda and Boyce, 1993), which is widely used in computational simulations, are

$$B_i = \frac{1}{3} C^R \sqrt{N} \frac{V_i^2 - \lambda^2}{\lambda} L^{-1}\left(\frac{\lambda}{\sqrt{N}}\right),$$

$$L(x) = \coth x - \frac{1}{x}, \quad \lambda^2 = \frac{1}{3}(V_1^2 + V_2^2 + V_3^2), \tag{2}$$

where B_i is the principal component of back-stress, V_i is the principal plastic stretch, $\lambda_L = \sqrt{N}$ is the locking stretch, i.e., limiting stretch in tension, N is the average number of segments in a single chain, $C^R = nkT$ is a constant, n is the number of chains per unit volume, k is Boltzmann's constant, and L is the Langevin function. In the eight-chain model (Arruda and Boyce, 1993) and other models (Boyce et al. 1988, Wu and Van der Giessen 1993), the number of entangled points of molecular chains is assumed to be fixed during the deformation, and the average number of segments, N, is constant. Therefore, these models are referred to as affine models. To accommodate the change in the entanglement situation due to deformation and temperature change (Raha and Bowden, 1972, Botto et al. 1987) , a nonaffine model (Tomita et al. 1997, Tomita and Adachi 1998) in which the change in the number of entangled points is taken into account, has been proposed. The simplest expression of the number of entangled points m in the temperature-independent case becomes

$$m(\xi) = m_0\{-c(1-\xi)\}. \tag{3}$$

The variable ξ representing the local deformation of polymeric material that reflects the change in the relative angle of the coordinate axes with unit base vectors g_i which are embedded parallel to the directions of principal plastic stretch in the initial stage of plastic deformation and deform into G_i with subsequent deformation. For volume-constant deformation, $\xi = 1/(|G_1||G_2||G_3|)$. m_0 is the number of entangled points at the reference temperature $T = T_0$ and the initial state of deformation $\xi = 1$. c is a material constant. The decrease in ξ causes a reduction in the number of entangled points m. Correspondingly, the average number of segments in a single chain increases, which results in enhanced extensibility of the materials.

The three-dimensional constitutive equation in updated Lagrangian formulation can be derived along the same lines as discussed by Boyce et al. (1988), in which the plastic strain rate is assumed to be parallel to the deviatoric part of driving stress $\hat{\sigma}_{ij} = \sigma_{ij} - B_{ij}$ where σ_{ij} is

the Cauchy stress and B_{ij} is the back-stress tensor with the principal values B_i in Eq. (2).

The plastic strain rate $\dot{\varepsilon}_{ij}^{p}$ can be expressed as

$$\dot{\varepsilon}_{ij}^{p} = \frac{\dot{\gamma}^{p}}{\sqrt{2}\tau}\hat{\sigma}'_{ij} \ , \quad \tau = \left(\hat{\sigma}'_{ij}\hat{\sigma}'_{ij}/2\right)^{1/2} . \tag{4}$$

The shear strain rate $\dot{\gamma}^{p}$ is estimated using Eq. (1), while τ in Eq. (1) is determined by using Eq. (4). The complete elastoplastic constitutive equation can be established by introducing the constitutive equation for the elastic part of the strain rate. The final constitutive equation that relates the rate of Kirchhoff stress $\dot{S}_{ij}$ and strain rate $\dot{\varepsilon}_{kl}$ becomes

$$\dot{S}_{ij} = L_{ijkl}\dot{\varepsilon}_{kl} - P'_{ij}, \quad L_{ijkl} = D^{e}_{ijkl} - F_{ijkl}$$

$$F_{ijkl} = \frac{1}{2}\left(\sigma_{ik}\delta_{jl} + \sigma_{il}\delta_{jk} + \sigma_{jl}\delta_{ik} + \sigma_{jk}\delta_{il}\right), \quad P'_{ij} = L_{ijkl}\frac{\dot{\gamma}^{p}}{\sqrt{2}\tau}\hat{\sigma}'_{kl} , \tag{5}$$

where D^{e}_{ijkl} is the elastic stiffness tensor.

The material parameters for PC were given in (Tomita et al. 1997, Tomita and Adachi 1998) and are given in section 4.

3. Computational Strategies

In order to estimate the macroscopic deformation behavior of a blended polymer containing the second-phase, rubber particles that are assumed to be distributed periodically, the homogenization method (Guedes and Kikuchi, 1990) is extended, along the same lines as indicated for the viscoplastic case (Wu and Ohno, 1999), to the present problem described by an updated Lagrangian formulation (Hill, 1958, Kitagawa et al. 1972). Consider the two-dimensional problem shown in Fig.2, with domain Ω and boundary S subjected to surface force P_i on S_t and prescribed velocity on S_u. The body is formed by the spatial repetition of a base cell made of different materials. Assuming that the base cell is very small, of order η compared with the dimensions of the entire body, and the global coordinate is x_i for the whole body and the local coordinate is y_i related to the single base cell, then $y_i = x_i/\eta$. Similar to the assumption used in the case of linear elastic materials (Guedes and Kikuchi, 1990), the velocity v_i is presumed to be expressed as an asymptotic expansion with respect to parameter η. Substituting these into the virtual work principle . (Hill, 1958, Kitagawa et al. 1972) and rearranging at the same order η, we arrive at the homogenized expression of the virtual work principle.

$$\int_{\Omega}\left[L^{H}_{ijkl}\dot{E}^{0}_{kl}(\boldsymbol{v}) - P^{H}_{ij} + \sigma^{H}_{ij} + \tau^{H}_{ijkl}\frac{\partial v^{0}_{k}}{\partial x_l}\right]\frac{\partial \delta v_i}{\partial x_j}d\Omega = \int_{S_t}\dot{P}_i\delta v_i dS \tag{6}$$

$$\left.\begin{aligned}
L_{ijkl}^{H} &= \frac{1}{|Y|}\int_{Y}\left[L_{ijkl}-L_{ijpq}\frac{1}{2}\left(\frac{\partial\chi_{p}^{kl}}{\partial y_{q}}+\frac{\partial\chi_{q}^{kl}}{\partial y_{p}}\right)\right]dY \\
P_{ij}^{H} &= \frac{1}{|Y|}\int_{Y}\left[P_{ij}'-L_{ijkl}\frac{1}{2}\left(\frac{\partial\phi_{k}}{\partial y_{l}}+\frac{\partial\phi_{l}}{\partial y_{k}}\right)\right]dY, \\
\sigma_{ij}^{H} &= \frac{1}{|Y|}\int_{Y}\sigma_{mj}\frac{\partial\phi_{i}}{\partial y_{m}}dY, \\
\tau_{ijkl}^{H} &= \frac{1}{|Y|}\int_{Y}\left[\sigma_{lj}\delta_{ki}-\sigma_{mj}\frac{\partial\chi_{i}^{kl}}{\partial y_{m}}\right]dY.
\end{aligned}\right\} \tag{7}$$

$$\dot{\varepsilon}_{ij}^{0}(\boldsymbol{x},\boldsymbol{y}) = \dot{E}_{ij}^{0}(\boldsymbol{v})-\frac{1}{2}\left(\frac{\partial\chi_{i}^{kl}}{\partial y_{j}}+\frac{\partial\chi_{j}^{kl}}{\partial y_{i}}\right)\dot{E}_{kl}^{0}(\boldsymbol{v})+\frac{1}{2}\left(\frac{\partial\phi_{i}}{\partial y_{j}}+\frac{\partial\phi_{j}}{\partial y_{i}}\right) \tag{8}$$

$$\dot{S}_{ij}^{0}(\boldsymbol{x},\boldsymbol{y}) = L_{ijkl}\dot{\varepsilon}_{kl}^{0}(\boldsymbol{x},\boldsymbol{y})-P_{ij}' \tag{9}$$

Equations (6), (7) and (8), (9) are the governing equations for the macroscopic and microscopic scales, respectively. The notation $\dot{E}_{ij}^{0}$ indicates the macroscopic strain rate and χ^{kl} and ϕ are characteristic functions defined in the unit cell, which satisfy the Y periodicity and are determined by the following equations.

$$\int_{Y}\left[L_{ijpq}\frac{1}{2}\left(\frac{\partial\chi_{p}^{kl}}{\partial y_{q}}+\frac{\partial\chi_{q}^{kl}}{\partial y_{p}}\right)+\sigma_{qj}\delta_{pi}\frac{\partial\chi_{p}^{kl}}{\partial y_{q}}\right]\frac{\partial\delta v_{i}}{\partial y_{j}}dY = \int_{Y}\left(L_{ijkl}+\sigma_{lj}\delta_{ki}\right)\frac{\partial\delta v_{i}}{\partial y_{j}}dY \tag{10}$$

$$\boldsymbol{\chi}^{kl}\cdots \mathrm{Y-periodic}$$

$$\int_{Y}\left[L_{ijkl}\frac{1}{2}\left(\frac{\partial\phi_{k}}{\partial y_{l}}+\frac{\partial\phi_{l}}{\partial y_{k}}\right)+\sigma_{mj}\frac{\partial\phi_{i}}{\partial y_{m}}\right]\frac{\partial\delta v_{i}}{\partial y_{j}}dY = \int_{Y}P_{ij}'\frac{\partial\delta v_{i}}{\partial y_{j}}dY \tag{11}$$

$$\boldsymbol{\phi}\cdots \mathrm{Y-periodic}$$

Thus, characteristic functions χ^{kl} and ϕ for the unit cell depend solely on the material characteristics and configuration of the microstructure of the unit cell, which are, in turn, obtained without interacting stress and strain of the macroscale. On the other hand, the macroscopic equilibrium given by Eq. (6) can be solved independently because the macroscopic characteristic functions indicated in Eq. (7) are identified through Eq. (10) and (11). The homogenized material characteristics indicated by Eq. (7) reflect the volume fraction, size and distribution of second-phase-particle-dependent onset and propagation of the shear band in the unit cell. Once the average stress rate is estimated, different types of stress rate can be obtained using the same transformation rule on the micro-scale (Ohno and Okumura, 1999).

4. Computational Model

Figure 1 shows a typical rubber-blended polycarbonate (PC), where black circles represent the rubber particles which are spherical with μm length scale and are dispersed throughout the matrix (The Society of Polymer Science, Japan, 1991). The mechanical characteristics and damage of the blended material are strongly dependent on the initiation and propagation of the shear band in the matrix polymer and the cavitations of rubber particles, which are strongly affected by the volume fraction and size of rubber particles. Although the distribution of the rubber particles is somewhat random and this randomness has been investigated employing representative element method with many heterogeneous particles of random distribution (Smit et al. 1999) here, we assume that it is periodic and evaluate the detailed characteristics of microscopic deformation and clarify their effect on the macroscopic mechanical characteristics and damage due to crazing of the blended polymer.

Figure 3 illustrates the computational model in which rubber particles with radii of curvature of r_1 and r_2 are assumed to be distributed periodically. Here, the matrix satisfies the constitutive equation (5) and rubber particles satisfy that of isotropic elastic material. Each quadrilateral corresponds to a cross-triangular element. As indicated in Fig. 3, in the present investigation, the rubber particle is assumed to be a circular with radius of curvature contained in the unit cell with side lengths w_0 and l_0, which characterizes the cases that will be investigated. The boundary conditions on the macroscopic scale are that the upper and bottom surfaces are shear free with a constant displacement constraint, whereas the right and left surfaces are assumed to be stress free. In order to investigate the effect of the loading direction with respect to the principal direction of the unit cell, namely, the y_2 coordinate, the angle θ, which is the angle of the tension direction with respect to the principal direction of the unit cell, is introduced and is parametrically varied from 0 to 45 degrees. The cohesive interface condition between the matrix and rubber particles is assumed throughout the deformation processes. It is important to note that the constitutive models used do not have a material length scale. Thus, the only length scales in the problem are the cell dimensions which govern the solution through the dimensionless variables r_1 / r_2, l_0 / w_0 and volume fraction f_0.

Here we will discuss the effects of volume fraction f_0, the size of rubber particles r_1 / r_2 with $l_0 / w_0 = 1$ and the direction θ on such macroscopic deformation behavior as the average stress-strain relation and microscopic deformation behavior such as onset and propagation of the shear band, mean stress distribution in and outside of particles, and the normal stress along the interface.

For a typical unit cell, which is the microscopic element of the blended material, a macroscopically homogeneous strain rate with average strain rate $\dot{\varepsilon}_0 = 0.0001/s$ is applied. The material parameters for the rubber-blended PC employed are $E / s_0 = 23.7$, $s_{ss} / s_0 = 0.79$, $h / s_0 = 5.15$, $As_0 / T_0 = 78.6$, $\alpha = 0.08$, $\dot{\gamma}_0 = 2.0 \times 10^{15} / s$, $s_0 = 97 MPa$, $T_0 = 296K$, $m_0 = 7.83 \times 10^{26}$ and $c = 0.33$ (Tomita et al. 1997, Tomita and Adachi 1998) which were the modified version

of those for affine-type 8-chain model (Arruda and Boyce, 1993, Wu and Van der Giessen 1993). The rubber particles are assumed to behave elastically with 0.05 times the elasticity modulus of a glassy polymer. This elasticity modulus is estimated so as to express the initial value of that for rubber.

5. Computational Results and Discussions

Here, the problems associated with the size and volume fraction of the rubber-particle-dependent microscopic to macroscopic deformation behavior of a blended polymer are investigated employing the computational model presented in section 4. Therefore, computational models with different mesh sizes are inevitable, so that the effect of mesh size on the results of computational simulation should be minimized. As far as the present problems are concerned, precise examination of the mesh sensitivity of the computationally obtained results confirmed that the simulated results are almost independent of the finite element discretization size employed.

5.1 Average stress-strain relations for unit cell

Figure 4 shows the typical homogenized stress-strain relations for the unit cells containing particle sizes of $r_1 / r_2 = 1, 2$ and volume fractions $f_0 = 0.2, 0.4$ under uniaxial tension with different directions $\theta = 0, 15, 30, 45^\circ$. The response in the case of identical particle size exhibits considerable anisotropy, especially in yield stress and around yield points, depending on the direction. Macroscopic yield stress and stress corresponding to the strain over yielding point for $\theta = 30^\circ, 45^\circ$ are higher than those for $\theta = 0^\circ, 15^\circ$. In contrast, it decreases for the case of different rubber particle size, $r_1 / r_2 = 2$ and is nearly isotropic for all deformation processes investigated here. It is noted that the macroscopic yield stress is essentially identical to this case. These typical characteristics are seen in the case with $r_1 / r_2 = 5$ in which, as opposed to the case for $r_1 / r_2 = 1, 2$, yield stress for $\theta = 0^\circ, 15^\circ$ is slightly higher than that for $\theta = 30^\circ, 45^\circ$. Due to the excessive deformation of the matrix, the computation was terminated at $u / L = 0.150$ for $r_1 / r_2 = 2$ with $\theta = 45^\circ$. The discussion concerning the stress-strain relation and the deformation characteristics in the unit cell will be given in section 5.2. These results suggest that the blending of particles of different sizes has a tendency to result in materials exhibiting macroscopically isotropic response. Regardless of the size difference of the particles, the increase of the volume fraction of rubber particles causes a considerable drop in the yield stress and suppresses the anisotropy in the response over the entire deformation range. Interestingly, over in a later stage of deformation, the resistance to deformation of the blended material approaches that of the matrix polymer, which is attributable to the contribution of blending to the promotion of orientation hardening in the ligament area of the matrix polymer.

5.2 Onset and propagation of shear band in unit cell

The equivalent strain rate distributions are shown in Fig. 5 with five different deformation levels of $u/L = 0.025, 0.050, 0.100, 0.150$ and 0.200. Fig. 5, where (a) $\theta = 0$ with $r_1 / r_2 = 1$, shows the typical onset and propagation behavior of the shear band. The high-strain-rate region emanating from the equator of the particle and matrix area localizes into a "wing"-type shear band, as called by Steenbrink and van der Giessen (1997, 1998) and then develops. The corresponding stress strain relation in Fig.4 (a) exhibits an inflection at the point where the wing-type shear band developed. Subsequently, the orientation hardening in the core of the shear band starts to harden so that the rate of deformation at the center of the band decreases. The front of the sheared region advances as multibands of high strain rate, and propagates towards upper and lower sides of the matrix. For the case with $\theta = 15^\circ$, a very strong shear band that connects the particles appears with relatively small deformation, which is attributable to the decrease of the yield points, as indicated in Fig.4 (a). Then the front of the sheared region advances as two bands to undeformed regions while preserving the same pattern. Increasing the angle to $\theta = 30^\circ$, high-strain-rate regions appear near the surface of the particles and they connect with the nearest particles at 45 degrees with respect to the tension direction, and subsequently, a new very strong shear band at 45 degrees with respect to the tension direction develops and connects particles. However, the intensity of the former shear band is weak as compared with the latter; this suppresses the large drop of yield stress, as shown in Fig.4 (a). Then they move along the particle surface and align. With further deformation, shear bands again start to misalign, which causes additional distortion of the particle. In the case of $\theta = 45^\circ$, the high-strain-rate regions appeared near the surface of the particle and the midpoint between two particles connect, forming the wing-type shear bands. In the later stage of deformation, for $\theta = 15,30^\circ$, the characteristic features of shear band patterns partially share those in the case of 0 and 45 degrees.

As can be seen in the strain rate distributions, the shear bands that connect particles and which developed in the early stage of deformation are attributable to the reduction of the macroscopic yield stress, as is observed in Fig.4. In the later stage of deformation, depending on the shear band development and propagation, there was the substantial rotation and distortion of the particle as can be seen in Figs. 6 and 7 that promoted the further development and propagation of the secondary shear band. All shear bands have a tendency to incline toward the tension direction at 45 degrees. Due to the reduction of the distance between the particles caused by the increase of the volume fraction of the particles, although the characteristic feature of the shear band developments is common with that in the case of low volume fraction, the shear band connecting the particles with reduced intensity becomes predominant. This tendency is also caused by the reduction of the stress concentration due to the increase of the radius of curvature of the particles.

The strain rate distribution in the case of different particle sizes is shown in Fig.5 (b). For 0 and 15 degrees, as indicated, wing-type shear bands emanate from the surface of the

small particle, whereas they start from the surface of large particles in the cases of 30 and 45 degrees. Subsequently, the shear band connects large particles via small particles. Most of the typical characteristic features of onset and propagation of the shear band in the case of uniformed particle size is preserved, except in the case of 30 degrees. Very complicated shear bands appeared in the case of 30 degrees. Initially, a shear band connecting large particle appears and subsequently, a new shear band connecting large particles via small particles develops. Due to orientation hardening, these bands move and propagate to the undeformed region. In the later stage of deformation, a very strong shear band connecting small particles develops. As we increase the size difference between particles to $r_1 / r_2 = 5$, most of the typical characteristic features for $r_1 / r_2 = 2$ are preserved. Within the range of deformation simulated in the present investigation, strong shear bands connecting small particles were not seen in the case of 30 degrees. The shear band connecting large particles via small particles was not seen in the case of 45 degrees. These different characteristic features results in the slight difference in the macroscopic yield stress, as mentioned in section 5.1, and in the macroscopic deformation behavior.

The deformation and rotation of the particles indicated in Figs.6 and 7 affects the shear localization and propagation. Fig. 7(b) clearly shows that the direction of rotation of large particles is opposite of same-sized particles and that small particles largely rotate in the opposite direction to that of large particles. The rotation of the particles is strongly affected by the connection of the shear band. Namely, for the rotation of the small particle shown in Fig.7 (b) for the 30 degrees case, the rotation rate drastically changes as different types of shear bands appear after $u / L = 0.150$, as shown in Fig. 5(b).

In the case of volume fraction $f_0 = 0.4$, the shear bands were much more localized within the ligament area regardless of the tension direction. The pattern of onset and propagation of shear bands was similar to that of the case with $f_0 = 0.2$, except for the case of 30 degrees with $r_1 / r_2 = 2$ in which the very strong shear band connecting the small particles disappears in the later stage of deformation. This is attributable to the decrease of the ligament width due to the increase of the volume fraction of the rubber particles. Correspondingly, distortion and rotation of the particles are suppressed.

5.3 Mean stress and normal stress with respect to the interface of particle distributions

According to the computational estimation of mean stress in matrix, regardless of the size and volume fraction of the particles and the direction of the tension, in the early stage of deformation, high positive mean stress appears near the boundary surface between a particle and the matrix located at the equator with respect to the tension direction. This area moves with the propagation of the shear band. For the quantitative comparison, the maximum values of mean stress normalized by shear strength s_0 for the different deformation stages are shown in Table 1 for $r_1 / r_2 = 1, 2, 5$ and $f = 0.2$. The maximum value of mean stress attains a very high value at macroscopic yield points and decreases due to softening and then again

increases due to orientation hardening. The effect of the size difference in particles on the value of maximum mean stress is not substantial, however, the decrease of volume fraction causes the increase of its values in the macroscopic yielding range.

The craze yield condition for polymeric materials is given as $\sigma_1 - \sigma_3 \geq A + B/\sigma_m$ where σ_1 and σ_3 are the maximum and minimum principal stresses, respectively, and A and B are the temperature-dependent material constants (Sterstein et al. 1968). Of necessity, mean stress σ_m must be positive to develop a stress state favorable for crazing. Although PC favors shear yielding, the positive mean stress in the matrix shown in Table 1 is an important characteristic value that governs the crazing of such materials as ABS and HIPS before the onset of cavitations in the particle.

The mean stress in the rubber particle is strongly related to the onset of cavitation. The maximum value of mean stress for $r_1/r_2 = 1$ depends on the direction of tension, and high values are attained with rather small deformation in 15- and 30-degree directions. On the other hand, due to the concentration of deformation in the early stage, maximum mean stress arises in large particles for 30- and 45-degree tension directions, whereas, it appears in small particles for 0- and 15-degree tension directions for $r_1/r_2 = 2$. These are reflected in the local distribution of the equivalent strain rate, as shown in Fig. 5. Furthermore, maximum values of mean stress for different-sized particles are higher than for identical-size particles. This tendency was enhanced as the size difference increased. It is noted that the increase in the volume fraction of particles causes a reduction of the maximum mean stress. Thus, it is proposed to introduce different-sized particles to promote the onset of cavitation, which would cause the reduction of the mean stress and in turn prevent the onset of damage due to crazing in the matrix.

Figure 8 shows the normal stress distribution along the interface between the matrix and rubber particles for the case with $r_1/r_2 = 2$, volume fraction of particles $f_0 = 0.2$ and tension directions $\theta = 0^\circ, 30^\circ$. To clearly show the relation between the location of the shear band and the point with high normal stress, the equivalent strain rate distributions are also shown in the same figure. The solid lines indicate normal stress and dotted lines stand for the equivalent plastic strain rate. Normal stress most notably affects the onset of debonding which causes cavitation of the particles and promotes the reduction of mean stress in the polymer matrix, contributing to the suppression of the onset of crazing. Due to the onset of the shear band and its propagation, very complex distribution patterns are observed. With regard to the maximum value of normal stress, as can be predicted based on the elasticity theory, the maximum value appears on the surface of small particles at the beginning of deformation, whereas the similar tendency for maximum mean stress is observed in a later stage of deformation, as is clearly seen in Table 2 of the maximum normal stress values on the surface of particles for $r_1/r_2 = 1, 2, 5$ and $f = 0.2$. The increase of deformation causes the shift of the high-strain-rate region to the north and south poles, accompanied by the high-normal-stress region. An interesting point is that the maximum values of normal stress are attained on the

boundary of small particles. These values increased as the size difference increased and the volume fraction decreased. Therefore, the present results suggest that the onset of debonding is promoted with increasing size difference and decreasing volume fraction of particles within the present simulations.

6. Conclusions

The problems associated with the tension-direction-dependent macro- to microscopic features of deformation of a blended polymer containing cylindrical rubber particles distributed periodically under the plane strain condition have been investigated. To simplify the problem, coherent conditions over the boundary of the matrix and rubber particles are assumed. A new homogenization method has been developed for the present problems. The onset and propagation of the shear band in the matrix, the mean stress distribution in the polymer matrix and particles, and the normal stress on the surface of rubber particles have been discussed in conjunction with the onset of cavitation in the particles and debonding over the interface. The results are summarized as follows.

(1) Depending on the tension direction with respect to the unit cell, different types of shear bands are observed. The shear band connecting the particles, which appeared in the early stages of deformation causes softening and thus is responsible for the decrease of the macroscopic yield stress. The onset of multi-shear bands contributes the distribution effect of strain.

(2) Increasing the volume fraction of rubber particles causes yielding of the polymer matrix in the early stage of deformation so that the macroscopic yield stress and the directional dependence of the macroscopic stress-strain relation decrease.

(3) The blended polymer with different-sized rubber particles shows very complex and different types of shear bands. Nevertheless, the macroscopic deformation behaviors are almost isotropic, which is due to the small particles that contribute to the high stress concentration, and promote the onset and propagation of the shear band.

(4) The decrease of the volume fraction of particles causes an increase of the maximum value of mean stress in the matrix around the macroscopic yielding range, whereas it is rather insensitive to the tension direction.

(5) The increase of the size difference and decrease of the volume fraction of particles cause the increases in maximum mean stress in particles and normal stress on the interface of particles. Therefore, these promote the onset of cavitation in particles and debonding along the interface of particles and suppress the onset of damage due to crazing in the matrix, which in turn promotes shear deformation.

Acknowledgements

Financial support from the Ministry of Education, Science, Sports and Culture of Japan is gratefully acknowledged. I wish to thank Idemitsu Kosan Ltd. for providing the

materials.

References

Adachi, T., Tomita, Y., and Kashu, Y., 1998. Trans. JSME, 64A: 758-764. (In Japanese)

Argon, A. S., 1973. Phil. Mag. 28: 839-865.

Arruda, E. M. and Boyce, M. C., 1993. J. Mech. Phys. Solids, 41:389-412.

Botto, P. A., Duckett, R. A. and Ward, I. M., 1987. Polymer, 28: 257-262.

Boyce, M. C., Parks, D. M. and Argon, A. S., 1988. Mech. Mater., **7:**15-33.

Fukui, T., Kikuchi, Y., and Inoue, T. 1991. Polymer, 32: 2367-2371.

Guedes, J. M., and Kikuchi, N. 1990. Comput. Meth. Appl. Mech. Engng., 83: 143-198.

Harward, R. N. and Thackray, G., 1968. Proc. R. Soc. Lond., A302: 453-472.

Hill, R., 1958. J. Mech. Phys. Solids, 10: 236-249.

Kashu, Y., Adachi, T. and Tomita, Y., 1996. Eds. Abe, T and Tsuta, T, Proc. AEPA'96 Pergamon, : 501-505.

Kitagawa, H, Seguchi, Y. and Tomita, Y., 1972. Ing. Arch., 41: 213-224.

Ohno, N. and Okumura, D., 1999. Proc. JSME. M&M99 Conference,239-240 (in Japanese)

Raha, S. and Bowden, P. B., 1972. Polymer, 13:174-183.

Smit, R. J. M., Brekelmans, W. A. M., and Meijer, H. E. H. 1999. J. Mech. Phys. Solids, 47: 201-221.

Socrate, S., and Boyce, M. C., 2000. J. Mech. Phys. Solids, 48: 233-273.

Steenbrink, A. C. and Van der Giessen, E. 1997. J. Mech. Phys. Solids, 45:405-437.

Steenbrink, A. C., and van der Giessen, E., 1998. De Borst, R and Van der Giessen, E., eds. Proc. IUTAM Symposium on Materials Instabilities, Wiley & Sons Ltd.:287-302.

Steenbrink, A. C., and van der Giessen, E., 1999. J. Mech. Phys. Solids, 47: 843-876.

Sterstein, S. S., Ongchin, L., and Silverman, A., 1968. Appl. Polym. Symp., **7:** 175-199.

Tanaka, S., Tomita, Y., and Lu, W., 2000. Trans. JSME. 66A: 454-463 (in Japanese)

The Society of Polymer Science, Japan Eds. 1991. High Performance Polymer Alloy, Maruzen Ltd. : 215-237.

Tomita, Y., Adachi, T., and Tanaka, S., 1997. Eur. J. Mech. A/Solids, 16: 745-755.

Tomita, Y. and Adachi, T., 1998. De Borst, R and Van der Giessen, E., Eds. Proc. IUTAM Symposium on Materials Instabilities, Wiley & Sons Ltd.: 303-321.

Tomita, Y., Tanaka, S., and Lu, W., 1999. Eds. F. Ellyin and J. W. Provan. Proc. ICM8, Progress in Mechanical Behaviour of Materials, :1061-1066.

Wu, P. D. and Van der Giessen, E., 1993. J. Mech. Phys. Solids, 41:427-456.

Wu, X. and Ohno, N., 1999. Bruhns, O. T., and Stein E., Eds, IUTAM Symposium on Micro- and Macrostructural Aspects of Thermoplasticity, Kluwer Academic Publishers : 187-196.

Yee, A. F. 1977. J. Mater. Sci., 12: 757-765.

Figure Captions; Table Captions

Figure.1 SEM Observation of Rubber Blended PC (The Society of Polymer Science, Japan, 1991).

Figure.2 Relation between macroscopic region and unit cell.

Figure.3 Computational model.

Figure. 4 Nominal stress normalized by shear strength σ_t / s_0 versus nominal strain u / L_0 for different particle sizes and volume fractions $f_0 = 0.2, 0.4$.

Figure. 5 Equivalent plastic strain rate distributions for different deformation levels and tensional direction with different particle sizes for $f_0 = 0.2$. From the top $\theta = 0, 15, 30, 45^\circ$

Figure.6 Rotation and distortion of different sized particles under different directional tensions for $f_0 = 0.2$.

Figure. 7 Rotation α of different sized particles initially aligned to tension direction for $f_0 = 0.2$.

Figure. 8 Normal stress σ_n / s_0 and plastic strain rate $\dot{\varepsilon}^p / \dot{\varepsilon}_0$ distribution along the interface of matrix and particle for large particle (upper) and small particle (lower) for $r_1 / r_2 = 2$ and $f_0 = 0.2$. The length of arrows indicates the scale of the figure.

Table 1. Maximum values of mean stress σ_m / s_0 for $f_0 = 0.2$.

Table 2. Maximum values of normal stress σ_n / s_0 for $f_0 = 0.2$.

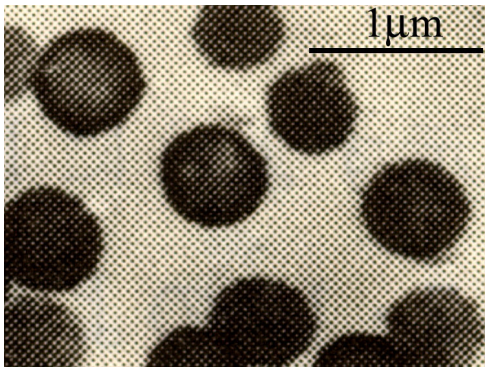

Figure.1 SEM Observation of Rubber Blended PC (The Society of Polymer Science, Japan, 1991).

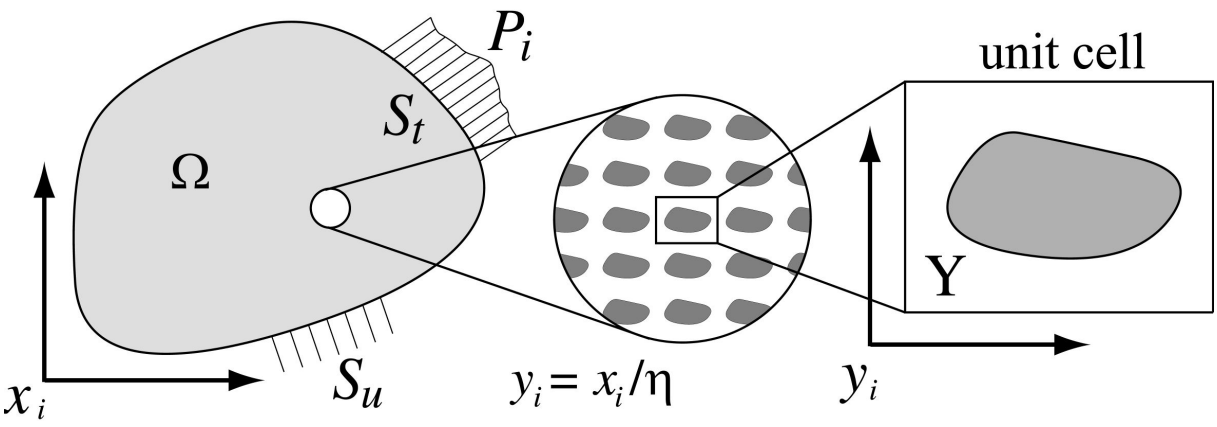

Figure.2 Relation between macroscopic region and unit cell.

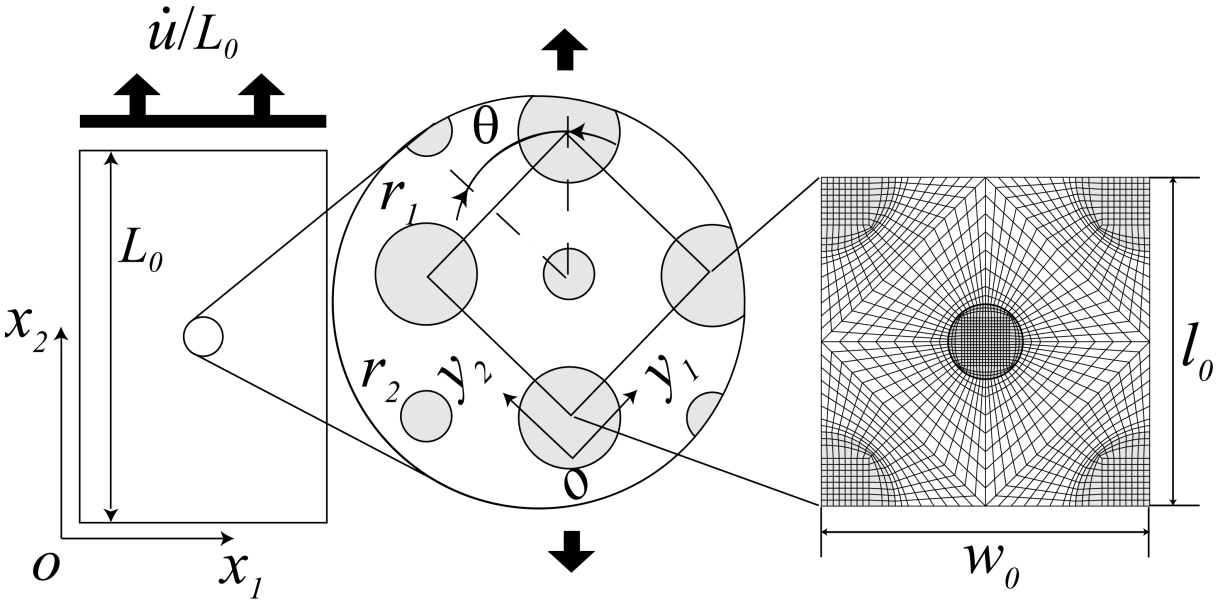

Figure.3 Computational model.

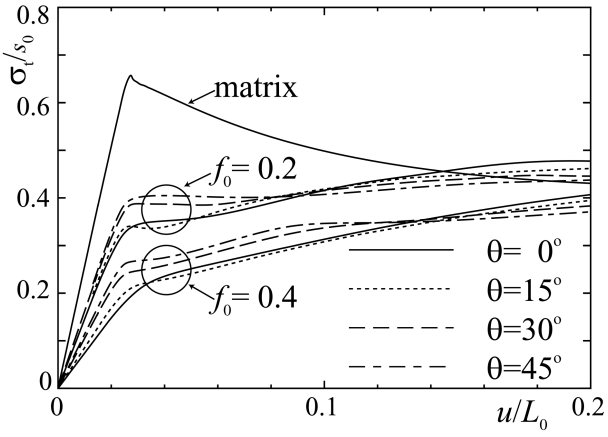

(a) $r_1 / r_2 = 1$

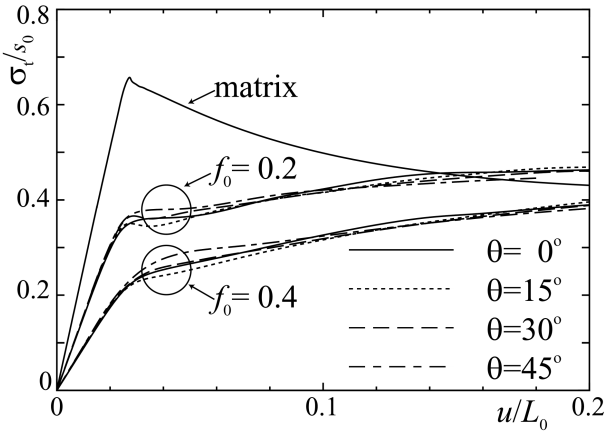

(b) $r_1 / r_2 = 2$

Figure. 4 Nominal stress normalized by shear strength σ_t / s_0 versus nominal strain u / L_0 for different particle sizes and volume fractions $f_0 = 0.2, 0.4$.

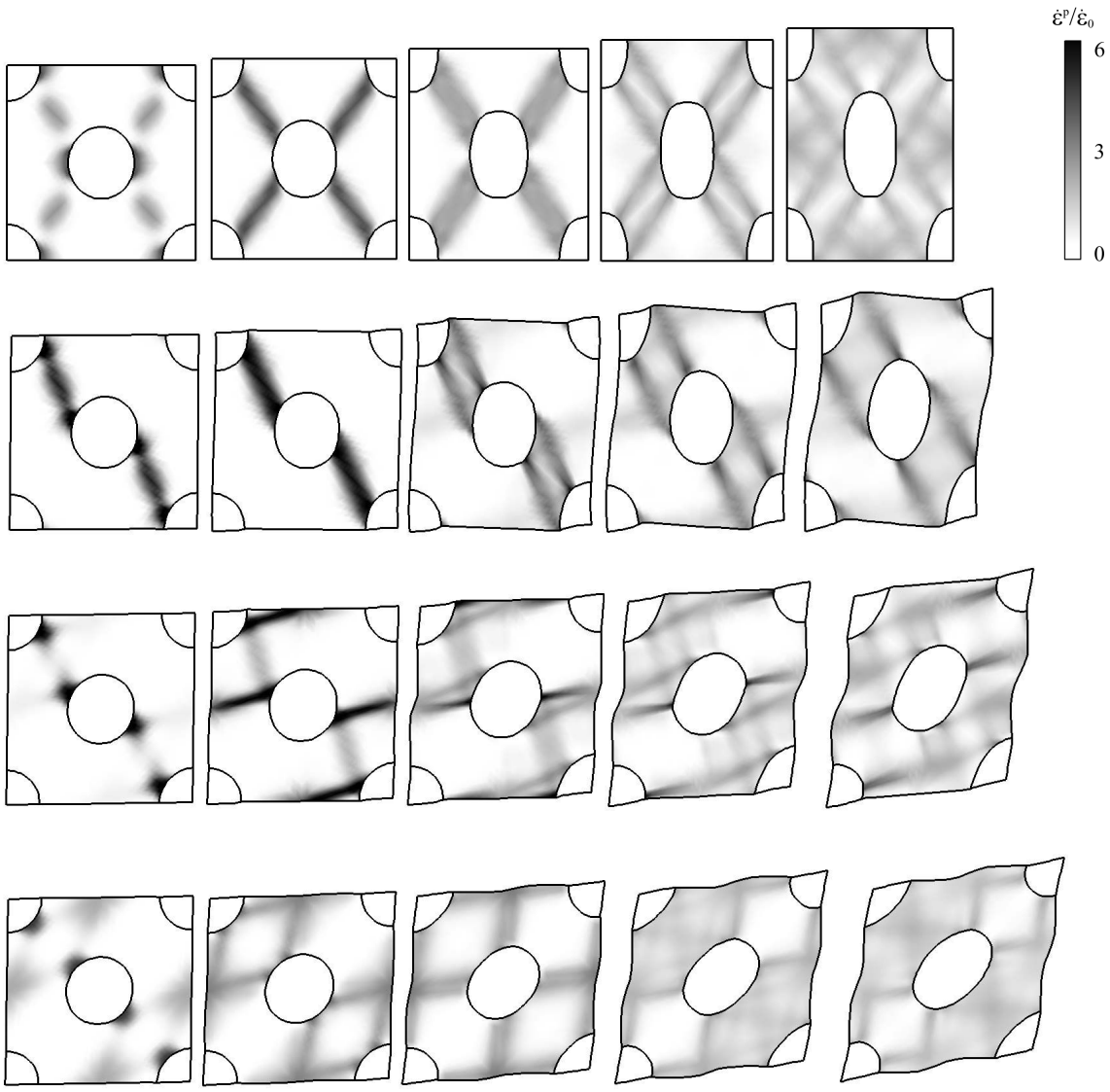

$u / L_0 = 0.025$ 0.050 0.100 0.150 0.200

(a) $r_1 / r_2 = 1$

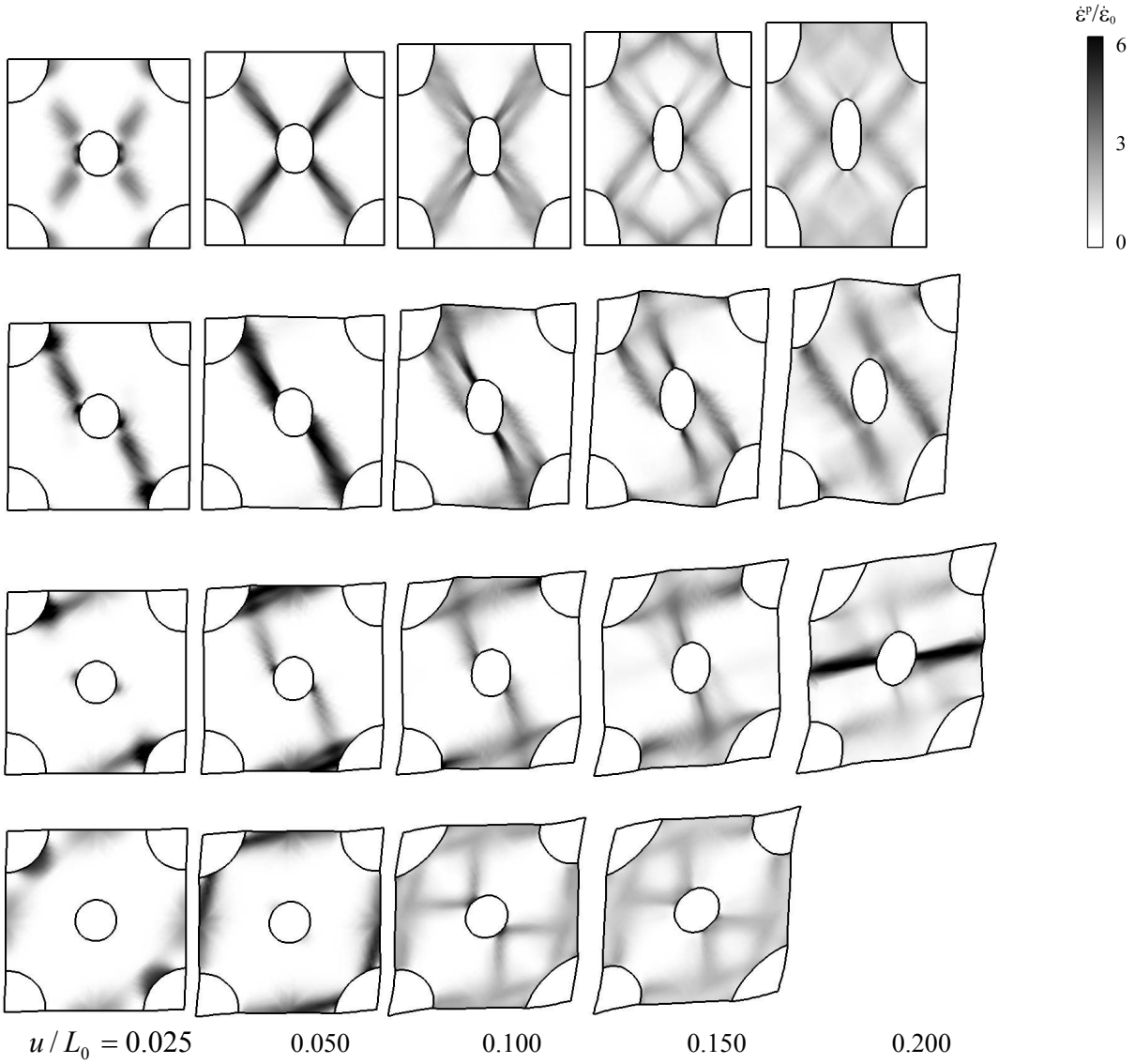

Figure 5 Equivalent plastic strain rate distributions for different deformation levels and tensional direction with different particle sizes for $f_0 = 0.2$. From the top $\theta = 0,\ 15,\ 30,\ 45^\circ$

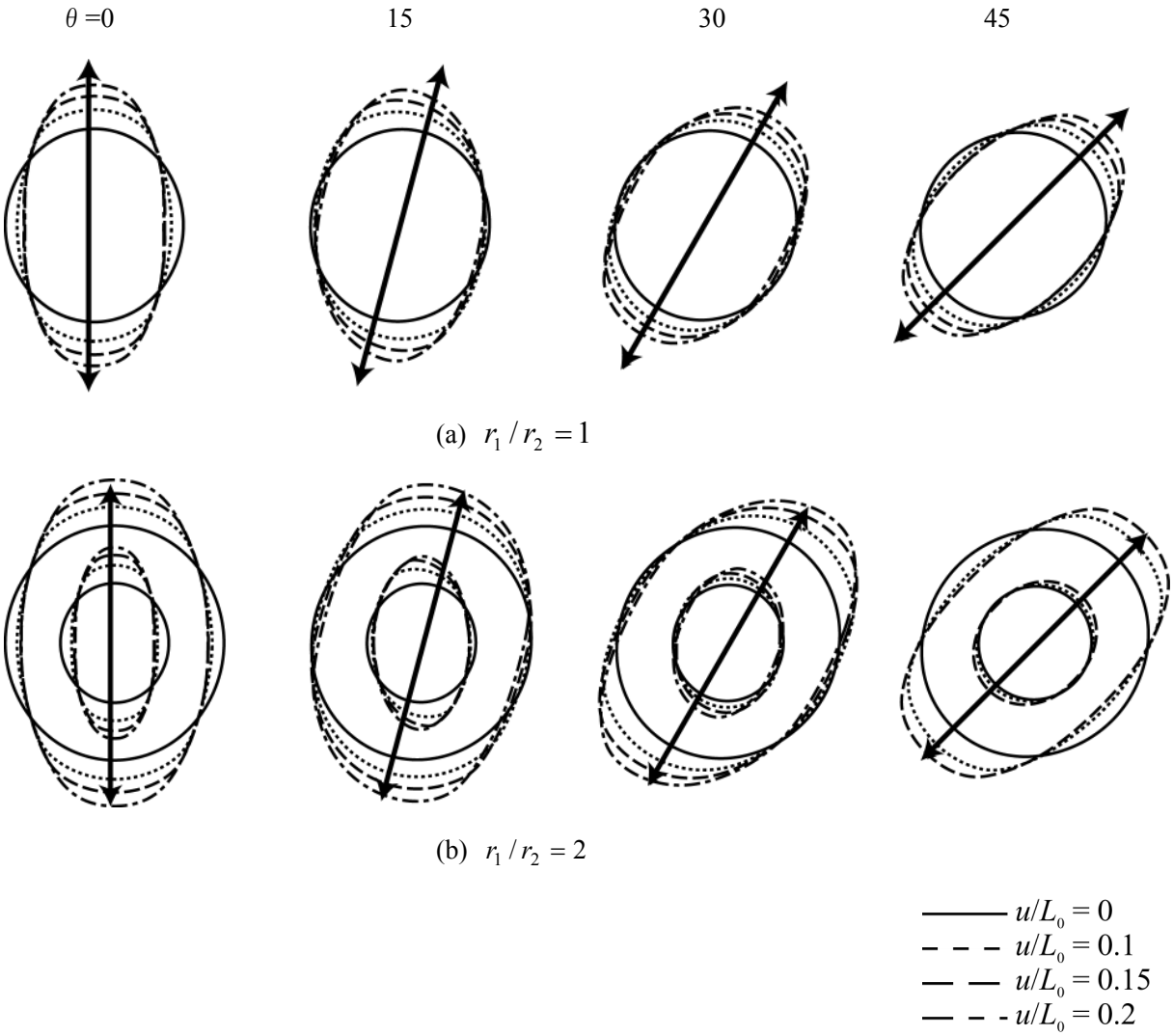

Figure.6 Rotation and distortion of different sized particles under different directional tensions for $f_0 = 0.2$.

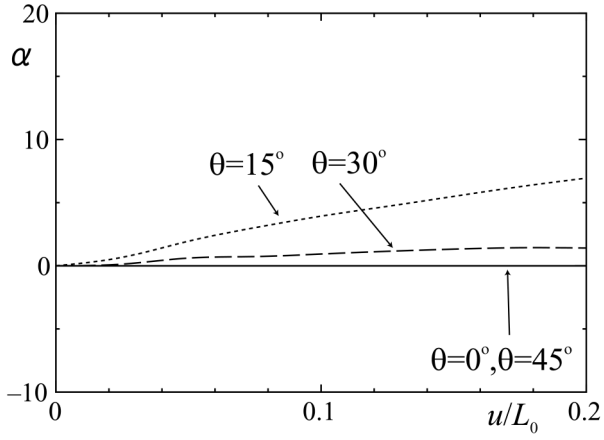

(a) $r_1 / r_2 = 1$

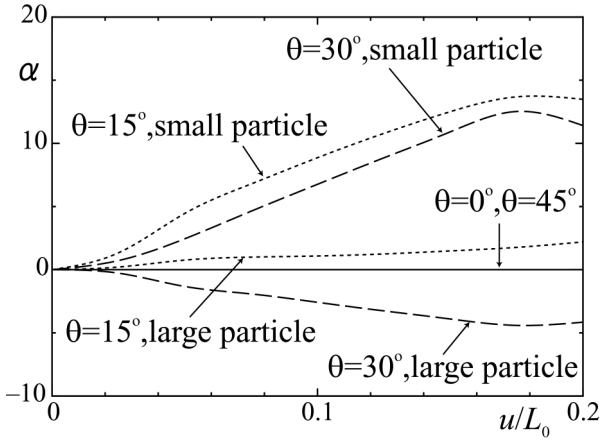

(b) $r_1 / r_2 = 2$

Figure. 7 Rotation α of different sized particles initially aligned to tension direction for $f_0 = 0.2$.

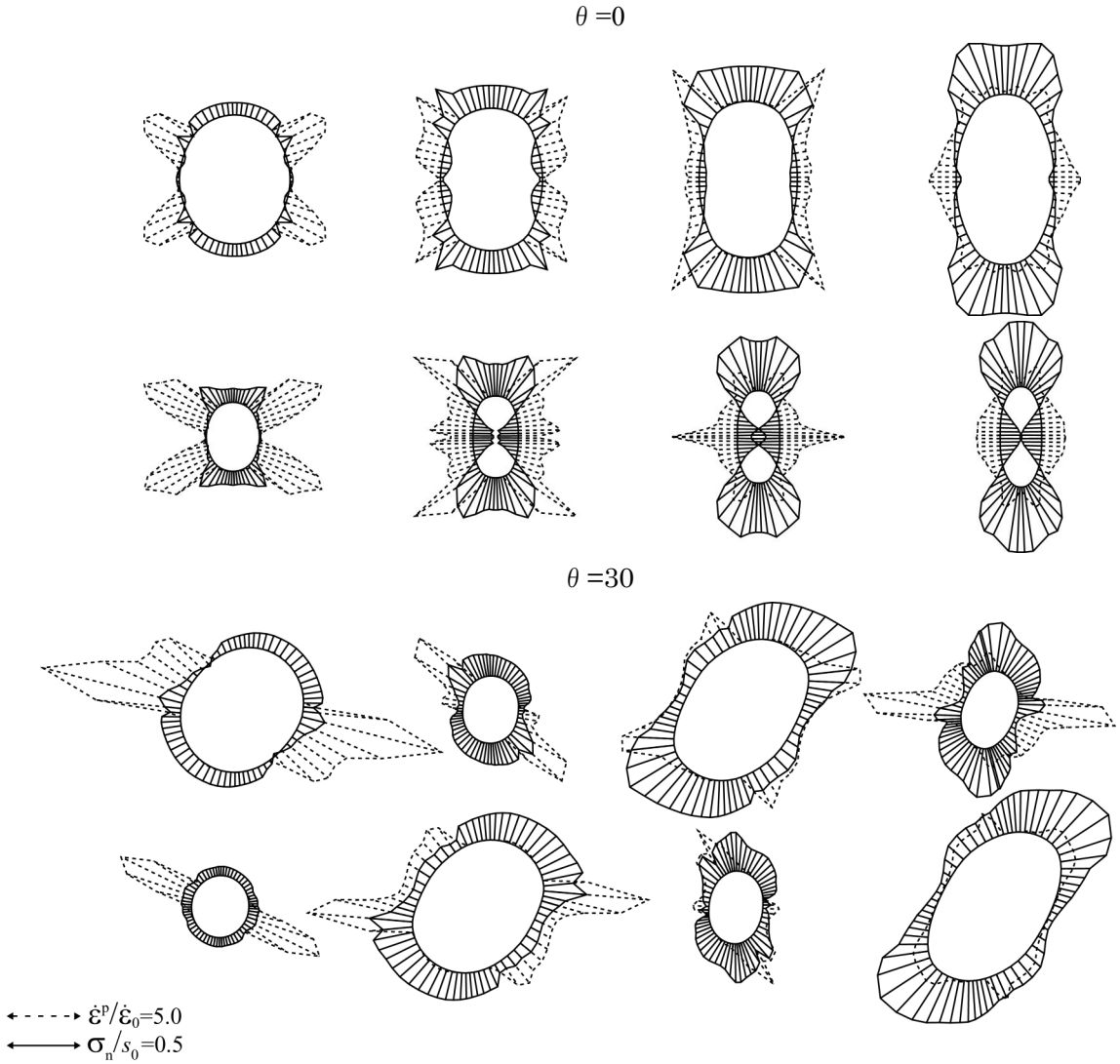

Figure. 8 Normal stress σ_n / s_0 and plastic strain rate $\dot{\varepsilon}^p / \dot{\varepsilon}_0$ distribution along the interface of matrix and particle for large particle (upper) and small particle (lower) for $r_1 / r_2 = 2$ and $f_0 = 0.2$. The length of arrows indicates the scale of the figure.

Table 1. Maximum values of mean stress σ_m / s_0 for $f_0 = 0.2$.

	θ \ u/L	0.025	0.050	0.100	0.200
r_1/r_2=1					
matrix	0	0.418	0.383	0.324	0.419
	15	0.443	0.401	0.488	0.456
	30	0.452	0.452	0.457	0.480
	45	0.443	0.466	0.375	0.380
particle	0	0.042	0.072	0.163	0.249
	15	0.052	0.165	0.261	0.280
	30	0.053	0.176	0.247	0.279
	45	0.049	0.092	0.143	0.235
r_1/r_2=2					
matrix	0	0.444	0.384	0.336	0.432
	15	0.451	0.424	0.479	0.473
	30	0.472	0.441	0.458	0.464
	45	0.468	0.432	0.460	
large particle	0	0.038	0.066	0.152	0.247
	15	0.051	0.149	0.246	0.293
	30	0.056	0.181	0.249	0.281
	45	0.052	0.087	0.152	
small particle	0	0.055	0.100	0.193	0.278
	15	0.057	0.171	0.249	0.267
	30	0.040	0.082	0.217	0.257
	45	0.033	0.044	0.131	
r_1/r_2=5					
matrix	0	0.454	0.431	0.390	0.443
	15	0.473	0.400	0.467	0.505
	30	0.454	0.454	0.449	0.450
	45	0.452	0.421	0.454	
large particle	0	0.044	0.066	0.153	0.222
	15	0.051	0.147	0.239	0.283
	30	0.052	0.174	0.250	0.278
	45	0.046	0.078	0.142	
small particle	0	0.066	0.182	0.250	0.236
	15	0.052	0.219	0.303	0.263
	30	0.031	0.041	0.201	0.254
	45	0.029	0.033	0.053	

Table 2. Maximum values of normal stress σ_n / s_0 for $f_0 = 0.2$.

	θ \ u/L	0.025	0.050	0.100	0.200
r_1/r_2=1					
	0	0.049	0.130	0.276	0.480
	15	0.055	0.196	0.340	0.514
	30	0.060	0.145	0.261	0.407
	45	0.061	0.113	0.247	0.410
r_1/r_2=2					
large particle	0	0.053	0.106	0.297	0.445
	15	0.058	0.165	0.363	0.493
	30	0.061	0.183	0.335	0.485
	45	0.061	0.149	0.313	
small particle	0	0.077	0.206	0.366	0.501
	15	0.082	0.239	0.412	0.505
	30	0.087	0.083	0.235	0.377
	45	0.076	0.081	0.118	
r_1/r_2=5					
large particle	0	0.055	0.124	0.228	0.398
	15	0.060	0.161	0.272	0.452
	30	0.061	0.169	0.305	0.485
	45	0.061	0.126	0.269	
small particle	0	0.183	0.236	0.463	0.596
	15	0.198	0.293	0.446	0.562
	30	0.162	0.194	0.215	0.333
	45	0.119	0.133	0.189	